JOURNAL OF PROPULSION AND POWER
Vol. 30, No. 5, September–October 2014

Assessing Turbomachinery Performance Sensitivity to Boundary Conditions Using Control Theory

Andre C. Marta*
Universidade de Lisboa, 1049 Lisbon, Portugal
and
Sriram Shankaran†
General Electric Global Research Center, Niskayuna, New York 12309

DOI: 10.2514/1.B35087

The adjoint method is extended to assess the sensitivity of turbomachinery performance with respect to inlet and exit boundary conditions. The derivation of the adjoint and sensitivity equations are briefly derived in general form, such that they can be applied to any set of flow-governing equations. In this paper, the Reynolds-averaged Navier–Stokes equations have been used, where the k-ω turbulence model has been selected. A compressor rotor blade test case is studied for verification and demonstration of the methodology. The adjoint-based sensitivities are verified using finite differences. The sensitivities of efficiency and pressure ratio with respect to the boundary condition parameters prescribed at each computational grid node at the inlet and exit faces of the blade passage are illustrated in the form of contour plots. Circumferentially averaged values and sensitivities demonstrate that fuller, more uniform profiles lead to improved performance, in line with basic thermodynamic principles. Two examples of modifying either inlet or exit boundary profiles, according to the sensitivity data obtained, show that performance tuning can be achieved. The sensitivity assessment approach presented is shown to be accurate and extremely efficient, while providing the designer with valuable information and insights to achieve a robust design.

Nomenclature

E	=	total energy
e	=	internal energy
h	=	enthalpy
k	=	turbulence kinetic energy
p	=	pressure
$\boldsymbol{q}$	=	vector of conservative variables
q_j	=	heat flux
$\boldsymbol{R}$	=	residual operator
s	=	blade spanwise coordinate
t	=	time
$\boldsymbol{u}$	=	vector of boundary conditions
u_i	=	mean velocity components
x_j	=	coordinate direction
Y	=	function of interest
α, β	=	tuning steps
γ	=	heat ratio
η	=	isentropic efficiency
μ	=	viscosity
μ_m	=	molecular (laminar) viscosity
μ_T	=	turbulent eddy viscosity
π	=	absolute total pressure ratio
ρ	=	density
τ_{ij}	=	viscous stress tensor
$\boldsymbol{\psi}$	=	adjoint vector
ω	=	specific dissipation rate

Received 15 July 2013; revision received 11 April 2014; accepted for publication 19 April 2014; published online 18 July 2014.

*Researcher, Instituto Superior Técnico, Center for Aerospace Science and Technology, Av. Rovisco Pais 1. Member AIAA.

†Researcher, Fluid Mechanics Laboratory, 1 Research Circle. Member AIAA.

I. Introduction

IN TURBOMACHINERY design, one of the most important goals is to improve performance, while meeting a number of requirements. From an aerodynamic perspective, this could, for instance, imply increasing efficiency or total pressure ratio of rotors or decreasing the total pressure loss of stators. Although most of the effort to accomplish this is by blade shaping and endwall contouring, the boundary conditions play an extremely important role.

If the flow is modeled by some high-fidelity form of the Navier–Stokes equations, not only the conditions at the inlet sections are critical to the solution, but also some conditions at the exit influence the upstream flow, as one would recall from the hyperbolic nature of the governing equations.

In either single-stage or multistage turbomachinery design, the optimal shape of the blades depends strongly on the boundary conditions, which are typically set to some nominal values that are kept frozen during the design process. However, design best practices include the study of turbomachinery performance under variation of the boundary conditions. Most of these studies have been primarily made in a test rig, but with the advent of powerful computational resources and trustful computational fluid dynamics (CFD) tools, they can now be reliably performed in a virtual world. Typically, the same CFD software used for design at nominal conditions is also used to perform off-design simulations, implying as many CFD runs as there are boundary parameters that need to be evaluated. However, this approach is computationally prohibitive when the number of boundary condition parameters becomes large, as is the case when the inlet and exit boundary conditions are specified in the form of a radial profile and one wishes to estimate the impact of each data point of that profile in the overall performance.

Assessing the robustness of turbomachinery performance can be posed as estimating the sensitivity of some figures of merit with respect to its inlet and exit boundary conditions. The focus is then on efficiently estimating the sensitivity (also designated as gradient) of the function of interest (or vector of functions) with respect to a very large number of parameters (also known as design variables), in flow problems modeled by complex governing equations. The control theory approach, also called the adjoint method, emerges as the best solution for this sensitivity analysis.

This paper focuses on extending the adjoint method to handle inlet and exit boundary condition profiles as design parameters, thus

providing an efficient way to account for variations on the performance of the turbomachinery due to the boundary conditions. The obtained adjoint-based gradient information of aerodynamic performance metrics can be used in many different ways by the designer. For instance, it can be 1) directly used to manually tweak the flow, 2) incorporated in an automatic gradient-based optimization design framework, or 3) used for uncertainty quantification in robust design.

II. Control Theory

The adjoint method has already been mathematically well documented by Giles and Pierce [1] and, being a semi-analytic method, it is capable of computing derivatives with the same precision as the quantity that is being differentiated.

Adjoint methods have been used to perform sensitivity analysis of partial differential equations (PDEs) for over three decades. These methods were first applied to optimal control problems and thereafter used to perform sensitivity analysis of linear structural finite element models. The first application to fluid dynamics was due to Pironneau [2]. The method was then extended by Jameson to perform airfoil shape optimization [3]. Later, its use in three-dimensional problems led to applications such as aerodynamic shape optimization of wings [4], aerostructural design [5], and even optimal plasma seeding [6]. Recent applications to turbomachinery include aerodynamic shape design optimization of blades [7,8] and endwalls [9] and coupled aerodynamic–aeroelastic blade design optimization [10]. In that regard, Marta et al. [11] exposed an interpretation of adjoint solutions for turbomachinery flows.

The adjoint method is extremely valuable because it provides a very efficient method to compute the sensitivity of a given function of interest with respect to many parameters by solving a system of equations of size equivalent to the governing equations of the flow. Typically, its main area of application has been shape optimization [12–14], using gradient-based algorithms, because having an efficient and accurate sensitivity analysis capability is very important in high-fidelity design frameworks.

With the increasing interest in the fields of robust design and uncertainty quantification, the control theory can be extended to handle inlet and exit boundary conditions as design parameters. Among other uses, this proposed extension should assist on the important topic of inlet distortion flow, namely, in estimating the performance penalty in transonic fans operating within nonuniform inlet flow [15].

The next sections lay out the theory devoted to this goal, when the flow problem is governed by a complex PDE.

A. Flow-Governing Equations

The governing equations used in the present work are the Reynolds-averaged Navier–Stokes (RANS) equations. In conservation form, the Navier–Stokes system of equations may be written in index notation as

$$\frac{\partial \rho}{\partial t} + \frac{\partial}{\partial x_j}(\rho u_j) = 0 \tag{1a}$$

$$\frac{\partial}{\partial t}(\rho u_i) + \frac{\partial}{\partial x_j}(\rho u_i u_j + p\delta_{ij} - \tau_{ji}) = 0, \qquad i = 1,2,3 \tag{1b}$$

$$\frac{\partial}{\partial t}(\rho E) + \frac{\partial}{\partial x_j}(\rho E u_j + p u_j - u_i \tau_{ij} + q_j) = 0 \tag{1c}$$

where ρ, u_i, and E are, respectively, the density, mean velocity, and total energy; τ_{ij} is the viscous stress and q_j is the heat flux.

A turbulence model needs to be used to model the Reynolds stresses. In this paper, a two-equation turbulence model was used, in particular, the k-ω model of Wilcox [16]:

$$\frac{\partial}{\partial t}(\rho k) + \frac{\partial}{\partial x_j}(\rho k u_j) = \tau_{ij}\partial u_i \partial x_j - \beta_k \rho k \omega + \frac{\partial}{\partial x_j}\left[\left(\mu + \sigma_k \frac{\rho k}{\omega}\right)\frac{\partial k}{\partial x_j}\right] \tag{2a}$$

$$\frac{\partial}{\partial t}(\rho \omega) + \frac{\partial}{\partial x_j}(\rho \omega u_j) = \frac{\gamma \omega}{k}\tau_{ij}\partial u_i \partial x_j - \beta_\omega \rho \omega^2 + \frac{\partial}{\partial x_j}\left[\left(\mu + \sigma_\omega \frac{\rho k}{\omega}\right)\frac{\partial \omega}{\partial x_j}\right] \tag{2b}$$

where k is the turbulence kinetic energy and ω is the specific dissipation rate. The turbulent eddy viscosity is computed from $\mu_T = \rho k/\omega$ and the constants are $\gamma = 5/9, \beta_k = 9/100, \beta_\omega = 3/40$, $\sigma_k = 1/2$, and $\sigma_\omega = 1/2$. The effective viscosity used in the Navier–Stokes Eqs. (1a–1c) is then computed as $\mu = \mu_m + \mu_T$, where μ_m is the molecular (laminar) viscosity.

In semidiscrete form, the RANS governing Eqs. (1) and (2) can be expressed as

$$\frac{\mathrm{d}\boldsymbol{q}_{ijk}}{\mathrm{d}t} + \boldsymbol{R}_{ijk}(\boldsymbol{q}) = 0 \tag{3}$$

where $\boldsymbol{q} = (\rho, \rho u_i, \rho E, \rho k, \rho \omega)^T$ is the vector of conservative variables, $\boldsymbol{R}$ is the residual with all of its components (inviscid, viscous, and turbulent fluxes, boundary conditions, and artificial dissipation), and the triad ijk represents the three computational directions. The unsteady term of Eq. (3) is dropped out because only the steady solution of the equation is of interest in this work.

B. Adjoint Equations

For the derivation of the adjoint equations for systems of PDEs, a Lagrangian viewpoint is used. This approach follows the method of Lagrange multipliers for the solution of a constrained minimization problem, in which the augmented function of interest is defined as

$$\tilde{Y}(\boldsymbol{q}, \boldsymbol{u}) = Y(\boldsymbol{q}, \boldsymbol{u}) - \boldsymbol{\psi}^T \boldsymbol{R}(\boldsymbol{q}, \boldsymbol{u}) \tag{4}$$

where $\boldsymbol{\psi}$ is the vector of Lagrange multipliers that takes the role of the adjoint variables, and $\boldsymbol{u}$ is the vector of design variables, which here are the inlet and exit boundary condition parameters. From the definition of augmented function of interest, the constraints are naturally enforced by the optimal solution, thus the governing equations are automatically satisfied.

The sensitivity of the augmented function of interest is then

$$\frac{\mathrm{d}\tilde{Y}}{\mathrm{d}\boldsymbol{u}} = \frac{\mathrm{d}Y}{\mathrm{d}\boldsymbol{u}} - \boldsymbol{\psi}^T \frac{\mathrm{d}\boldsymbol{R}}{\mathrm{d}\boldsymbol{u}} \tag{5}$$

which can be expanded as

$$\frac{\mathrm{d}\tilde{Y}}{\mathrm{d}\boldsymbol{u}} = \left(\frac{\partial Y}{\partial \boldsymbol{q}}\frac{\mathrm{d}\boldsymbol{q}}{\mathrm{d}\boldsymbol{u}} + \frac{\partial Y}{\partial \boldsymbol{u}}\right) - \boldsymbol{\psi}^T\left(\frac{\partial \boldsymbol{R}}{\partial \boldsymbol{q}}\frac{\mathrm{d}\boldsymbol{q}}{\mathrm{d}\boldsymbol{u}} + \frac{\partial \boldsymbol{R}}{\partial \boldsymbol{u}}\right) \tag{6}$$

Rearranging Eq. (6) results in

$$\frac{\mathrm{d}\tilde{Y}}{\mathrm{d}\boldsymbol{u}} = \left(\frac{\partial Y}{\partial \boldsymbol{q}} - \boldsymbol{\psi}^T \frac{\partial \boldsymbol{R}}{\partial \boldsymbol{q}}\right)\frac{\mathrm{d}\boldsymbol{q}}{\mathrm{d}\boldsymbol{u}} + \left(\frac{\partial Y}{\partial \boldsymbol{u}} - \boldsymbol{\psi}^T \frac{\partial \boldsymbol{R}}{\partial \boldsymbol{u}}\right) \tag{7}$$

To eliminate the dependence on the flow variables, the term involving $\mathrm{d}\boldsymbol{q}/\mathrm{d}\boldsymbol{u}$ must vanish, which is achieved by choosing $\boldsymbol{\psi}$ such that it satisfies the adjoint equation

$$\frac{\partial Y}{\partial \boldsymbol{q}} - \boldsymbol{\psi}^T \frac{\partial \boldsymbol{R}}{\partial \boldsymbol{q}} = 0 \Rightarrow \left[\frac{\partial \boldsymbol{R}}{\partial \boldsymbol{q}}\right]^T \boldsymbol{\psi} = \left[\frac{\partial Y}{\partial \boldsymbol{q}}\right]^T \tag{8}$$

C. Adjoint-Based Sensitivities

Once $\boldsymbol{\psi}$ is obtained by solving the adjoint system of equations (8), the sensitivity of the function of interest with respect to the inlet or exit boundary conditions $\boldsymbol{u}$ set at each computational boundary face grid node is given by Eq. (5), which can be rewritten as

$$\frac{\mathrm{d}Y}{\mathrm{d}\boldsymbol{u}} = \frac{\partial Y}{\partial \boldsymbol{u}} - \boldsymbol{\psi}^T \frac{\partial \boldsymbol{R}}{\partial \boldsymbol{u}} \tag{9}$$

Equation (9) reveals the advantage of the adjoint approach (the independence of $\delta \boldsymbol{q}$), meaning that the gradient of Y with respect to an arbitrarily large vector of parameters $\boldsymbol{u}$ can be determined without the need for additional solutions of the PDE. This is in contrast with standard sensitivity analysis methods, such as finite difference approximations, that require a number of additional flow solutions proportional to the number of parameters.

It should be noted, however, that the evaluation of the sensitivity of each function of interest requires solving Eq. (8) with a new right-hand side vector. On the other hand, the computational cost of the function sensitivity Eq. (9) is almost independent of the number boundary parameters $\boldsymbol{u}$, which is the feature that makes the adjoint method so attractive for problems involving a large number of parameters and a few functions.

III. Implementation

The two center pieces included in the methodology presented in this paper are the flow solver and the adjoint solver. Given the maturity of CFD, the implementation of the flow solver is only briefly mentioned, being the main focus the development of the adjoint solver and its extension to the computation of sensitivities with respect to boundary conditions.

A. Flow Solver

The proprietary flow solver used in this work supports three-dimensional, multiblock, structured grids, and it uses a finite volume formulation of the steady and unsteady, nonlinear and linear RANS equations. Several turbulence models are available, such as k-ω, k-ε, and SST, having the option to use wall functions or wall integration for boundary-layer resolution. A detailed description of the numerical techniques employed can be found in [17–19]. This solver is typically employed in the solution of turbomachinery blade rows and it is capable of efficiently performing three-dimensional analysis for aeromechanics, aerodynamic design, parametric studies, and robust design applications.

As typical for most iterative CFD flow solvers, the residual calculation Eq. (3) is done in a subroutine that loops through the three-dimensional domain and accumulates the several fluxes and boundary conditions contributions in $\boldsymbol{R}$.

In this paper, the steady, nonlinear RANS equations with k-ω turbulence model [16], together with wall functions, are used.

The flow solver supports several inlet and exit boundary conditions, including pressure extrapolation, Riemann invariant, and two-dimensional nonreflecting boundaries for the inlet, and velocity extrapolation, Riemann invariant, and non-reflecting boundaries for the exit. Denote by the subscript 1 the ghost cell outside the computational domain and by the subscript 2 the first interior cell in the direction normal to the boundary face, as illustrated in Fig. 1.

The extrapolation schemes, selected for the inlet and exit boundaries in the test cases presented in this paper, assume isentropic flow and calorically perfect gas. In the ghost cells at the inlet boundary, with reference to the cell numbering convention exhibited in Fig. 1a, the pressure and conservative variables are set as

$$p_1 = \min(p_2, p_T^{\text{inlet}}) \tag{10a}$$

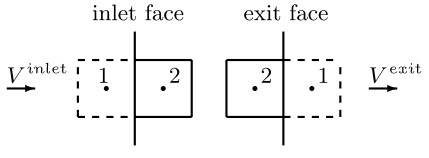

a) Inlet boundary **b) Exit boundary**

Fig. 1 Schematic of the computational cells at the boundaries.

$$\rho_1 = \rho_T \left(\frac{p_1}{p_T^{\text{inlet}}} \right)^{1/\gamma}, \qquad \rho_T = \frac{\gamma}{\gamma - 1} \frac{p_T^{\text{inlet}}}{h_T^{\text{inlet}}} \tag{10b}$$

$$(\rho u_x)_1 = \rho_1 [V_r \cos(\theta) - V_t \sin(\theta)], \quad V_r = V_{rz} C_r^{\text{inlet}}, \quad V_t = V_t^{\text{inlet}} \tag{10c}$$

$$(\rho u_y)_1 = \rho_1 [V_r \sin(\theta) + V_t \cos(\theta)] \tag{10d}$$

$$(\rho u_z)_1 = \rho_1 V_{rz} C_z^{\text{inlet}}, \qquad V_{rz} = \sqrt{V^2 - V_t^{2\text{inlet}}},$$
$$V^2 = 2(h_T^{\text{inlet}} - h^{\text{inlet}}), \qquad h^{\text{inlet}} = \frac{\gamma}{\gamma - 1} \frac{p_1}{\rho_1} \tag{10e}$$

$$(\rho E)_1 = \frac{1}{\gamma - 1} p_1 + \frac{1}{2} \rho_1 V^2 \tag{10f}$$

$$(\rho k)_1 = \rho_1 k^{\text{inlet}} \tag{10g}$$

$$(\rho \omega)_1 = \rho_1 \omega^{\text{inlet}} \tag{10h}$$

where the prescribed inlet quantities are the total pressure p_T^{inlet}, total enthalpy h_T^{inlet}, absolute tangential velocity V_t^{inlet}, radial direction cosine C_r^{inlet}, axial direction cosine C_z^{inlet}, and turbulence level through k^{inlet} and ω^{inlet}. The scheme selected for the exit prescribes the static pressure p^{exit}. The other quantities are extrapolated. This yields the following relations for the pressure and conservative variables in the ghost cells at the exit boundary, with reference to the cell numbering convention exhibited in Fig. 1b:

$$p_1 = p^{\text{exit}} \tag{11a}$$

$$\rho_1 = \frac{1}{\gamma - 1} \frac{p_1}{e_1}, \quad e_1 = E_1 - \frac{1}{2} V_1^2, \quad E_1 = E_2 = (\rho E)_2 / \rho_2 \tag{11b}$$

$$(\rho u_x)_1 = \rho_1 u_{x1}, u_{x1} = u_{x2} = (\rho u_x)_2 / \rho_2 \tag{11c}$$

$$(\rho u_y)_1 = \rho_1 u_{y1}, \qquad u_{y1} = u_{y2} = (\rho u_y)_2 / \rho_2 \tag{11d}$$

$$(\rho u_z)_1 = \rho_1 u_{z1}, \qquad u_{z1} = u_{z2} = (\rho u_z)_2 / \rho_2 \tag{11e}$$

$$(\rho E)_1 = \rho_1 \left(e_1 + \frac{1}{2} V_1^2 \right), \qquad V_1^2 = u_{x1}^2 + u_{y1}^2 + u_{z1}^2 \tag{11f}$$

$$(\rho k)_1 = \rho_1 (\rho k)_2 / \rho_2 \tag{11g}$$

$$(\rho \omega)_1 = \rho_1 (\rho \omega)_2 / \rho_2 \tag{11h}$$

The vector of boundary conditions $\boldsymbol{u}$ is then composed of $(p_T^{\text{inlet}}, h_T^{\text{inlet}}, V_t^{\text{inlet}}, C_r^{\text{inlet}}, C_z^{\text{inlet}}, p^{\text{exit}})$, where each of the six terms is of size corresponding to the number of ghost cells that discretize the block faces at the inlet or exit boundaries.

It should be noted that the flow solver reads prescribed radial profiles (one-dimensional) for inlet and exit boundary conditions, that is to say, it assumes circumferentially averaged values for the boundary faces. However, given the benefit of using the adjoint method, the sensitivities are computed with respect to the prescribed boundary values at every boundary cell face (two-dimensional surface), as detailed in Sec. III.B.

B. Adjoint Solver

The adjoint equations (8) for the RANS equations are obtained using a discrete formulation, where the governing PDE are first

discretized and then the adjoint system is derived from these discrete equations.

The discrete adjoint approach formulation is chosen because it can be applied to any set of governing PDEs and it can treat arbitrary functions of interest Y. As such, and in contrast to the continuous approach, no simplifications have to be made during the derivation: The effects of viscosity and heat transfer and the turbulence equations can be easily handled when deriving the discrete adjoint. Another advantage of this formulation is that the boundary conditions are handled seamlessly because the adjoint solver is derived from the discretized flow residual equations that already implement them. Therefore, the adjoint-based sensitivities computed are perfectly consistent with the flow solver.

The choice of the discrete approach makes it possible to use automatic differentiation (AD) tools to help build the adjoint solver routines. As such, the approach used in this work is a hybrid and it follows the work of Marta et al. [20]. The discrete adjoint solver is derived with the aid of AD, which is selectively applied to the CFD source code that handles the residual $\boldsymbol{R}$ and function Y evaluations. This hybrid approach retains the accuracy of the adjoint methods, while it adds the ease of implementation of the automatic differentiation methods.

The adjoint solver used has been built around the custom flow solver mentioned in Sec. III.A. The residual calculation in the iterative CFD solver is done in a subroutine that loops through the three-dimensional domain and accumulates the several fluxes and boundary conditions contributions in the residual $\boldsymbol{R}$. Applying a purely automatic approach to the nested-loop residual code would translate into enormous computational inefficiencies. Recognizing that the residual at each cell only depends on flow variables at that cell and at the cells adjacent to it, which define the stencil of dependence, the routines in the flow solver that evaluate the residuals were rewritten in such a way that the residual for a given computational cell R_{ijk} would be given by a routine of the form `subroutine residualAdj(ib, i, j, k, uAdj, qAdj, rAdj)`.

This routine returns the N_v residuals `rAdj`, given the stencil of boundary conditions `uAdj` and flow variables `qAdj` for a given node `(i, j, k)` in block `ib` on each processor. For the RANS equations, $N_v = 7$. There are a total of $(N_v \times N_s)$ flow variables in the stencil, where N_s is the dimension of the computational stencil used in the flow solver.

The AD tool chosen in this work is Tapenade [21] because it supports Fortran 90, which is a requirement taking into account the programming language used in the flow solver. Because of the way residuals are computed, the reverse mode is much more efficient in this case and, on this basis, it was used to produce adjoint code for the set of residual evaluation routines. The automatic differentiation process produced the differentiated routine `subroutine residualAdj_B(ib, i, j, k, uAdj, uAdjB, qAdj, qAdjB, rAdj, rAdjB)`, where `qAdjB` and `uAdjB` are the derivatives of the residual with respect to the stencil of flow variables $\boldsymbol{q}$ and boundary conditions $\boldsymbol{u}$, respectively. Therefore, this routine is able to compute all the necessary nonzero entries for the matrices $\partial \boldsymbol{R}/\partial \boldsymbol{q}$ and $\partial \boldsymbol{R}/\partial \boldsymbol{u}$, used in Eqs. (8) and (9), respectively. The $N_v \times (N_v \times N_s)$ sensitivities that need to be computed for each node, corresponding to N_v rows in the $\partial \boldsymbol{R}/\partial \boldsymbol{q}$ matrix, are readily computed by this automatically differentiated routine in reverse mode because it yields

$$\texttt{qAdjB(ii, jj, kk, n)} = \frac{\partial \boldsymbol{R}(i, j, k, m)}{\partial \boldsymbol{q}(i + ii, j + jj, k + kk, n)} \tag{12}$$

where the triad `(ii, jj, kk)` spans the stencil, m spans the number of governing equations N_v and n spans the N_v flow variables. The $N_v \times (N_b \times N_p)$ sensitivities, corresponding to N_v rows in the $\partial \boldsymbol{R}/\partial \boldsymbol{u}$ matrix, are given by

$$\texttt{uAdjB(l, n)} = \frac{\partial \boldsymbol{R}(i, j, k, m)}{\partial \boldsymbol{u}(l, n)} \tag{13}$$

where `l` spans the boundary face nodes N_b and n spans the different boundary parameters N_p.

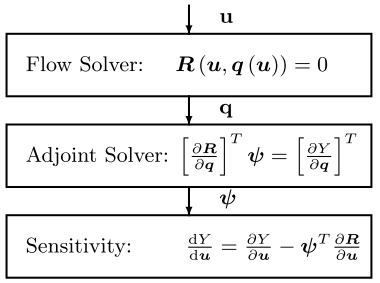

Fig. 2 Schematic of the adjoint-based BC sensitivity algorithm.

Similarly, the routine that evaluates the functions of interest is rewritten as `subroutine functionAdj(ib, i, j, k, uAdj, qAdj, yAdj)` and the AD tool produced the differentiated routine `subroutine functionAdj_B(ib, i, j, k, uAdj, uAdjB, qAdj, qAdjB, yAdj, yAdjB)`, which is used to evaluate the entries of the vectors $\partial Y/\partial \boldsymbol{q}$ and $\partial Y/\partial \boldsymbol{u}$, used in Eqs. (8) and (9), respectively.

This way, the code that computes the entries of the several matrices and vectors of partial derivatives necessary to evaluate gradients (9) using the adjoint method (8) is automatically generated. The sizes of the matrices and vectors involved in this process are

$$\frac{\partial \boldsymbol{R}}{\partial \boldsymbol{q}}(N_q \times N_q), \qquad \frac{\partial \boldsymbol{Y}}{\partial \boldsymbol{q}}(N_Y \times N_q),$$
$$\frac{\partial \boldsymbol{R}}{\partial \boldsymbol{u}}(N_q \times N_u), \qquad \frac{\partial \boldsymbol{Y}}{\partial \boldsymbol{u}}(N_Y \times N_u) \tag{14}$$

where N_Y is the number of functions of interest, N_u is the number of terms in the boundary condition (BC) stencil (number of BC parameters N_p times the number of boundary cell faces N_b), and N_q is the size of the state vector (number of governing equations N_v times the number of cells of the computational mesh). Although $\partial \boldsymbol{R}/\partial \boldsymbol{q}$ and $\partial \boldsymbol{R}/\partial \boldsymbol{u}$ can easily be very large matrices, they are extremely sparse as a consequence of the local stencil of dependence.

The large sparse linear system of adjoint equations (8) has to be solved N_Y times for different right-hand side vectors because $\boldsymbol{\psi}$ is valid for all boundary parameters $\boldsymbol{u}$ but must be recomputed for each function Y. The Portable, Extensible Toolkit for Scientific

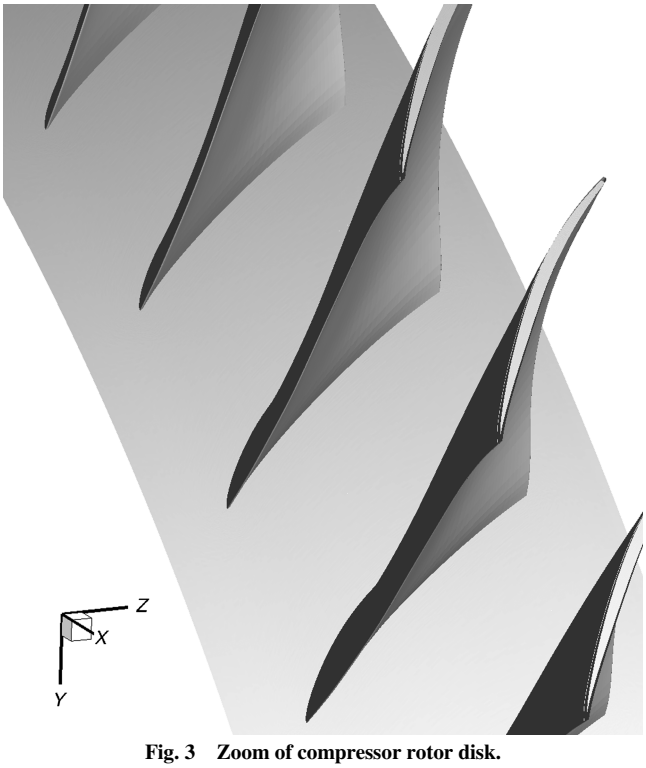

Fig. 3 Zoom of compressor rotor disk.

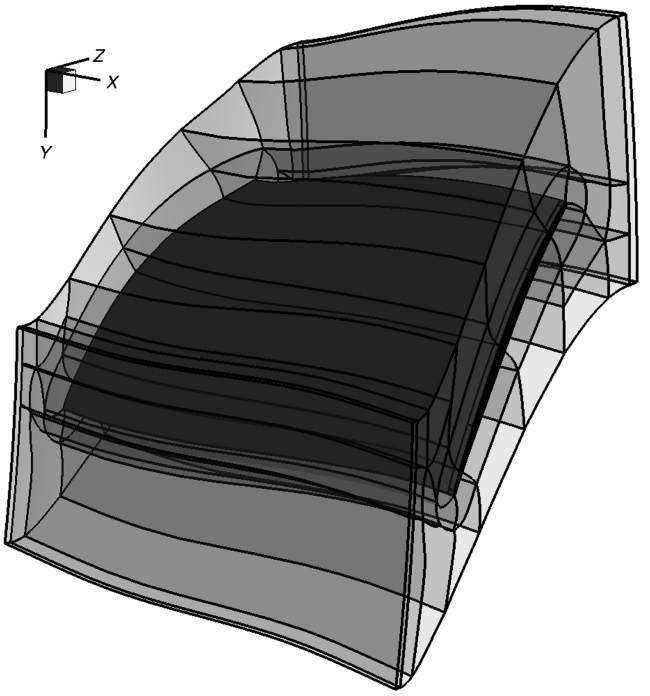

Fig. 4 Compressor rotor blade passage.

Computation [22] is used to solve the system. The Generalized Minimum Residual algorithm is used, preconditioned with the block-Jacobi method, with one block per processor, each solved with ILU (0) preconditioning.

The full RANS adjoint solver described makes use of the complete vector of conservative variables and handles the corresponding seven governing equations (1) and (2). Further details about the implementation and verification of the adjoint solver and the adjoint treatment of the turbulence equations can be found in the work of Marta et al. [23,24], respectively.

C. Performance Sensitivity to Boundary Conditions at Inlet and Exit

From a design perspective, the performance of turbomachinery depends heavily not only on the blade geometry but also on its inlet and exit boundary conditions. The algorithm proposed to assess the turbomachinery performance sensitivity to boundary conditions using control theory is illustrated in Fig. 2.

Let $\boldsymbol{u}$ denote the boundary condition at the inlet or exit sections. Given the mesh and the boundary conditions, the flow solver computes the flow solution $\boldsymbol{q}$ and, using some postprocessing, the values of the function of interest Y can easily be computed. Using the flow solution obtained from the flow solver, the adjoint solution $\boldsymbol{\psi}$ is evaluated using the adjoint solver. Once the adjoint solution is obtained from Eq. (8), the sensitivity of the function of interest with respect to the boundary conditions are computed by Eq. (9), which implies a simple matrix-vector multiplication operation.

IV. Results

The approach implemented in Sec. III has been applied to a representative test case: a transonic compressor rotor blade. The test comprises four parts: 1) the problem is described; 2) the flow and adjoint solutions are evaluated; 3) the adjoint-based sensitivities of the functions of interest are computed with respect to inlet and exit boundary conditions and verified against finite difference (FD) derivative approximations; and 4) a performance tuning example is used to demonstrate a possible use of the sensitivities computed.

A. Description of Test Case

The test problem is a transonic blade passage of a high-pressure axial compressor rotor. A zoom of the rotor wheel geometry is shown in Fig. 3, where the blade passage has been replicated for illustration purposes.

Only a single blade passage is modeled using periodicity. The mesh generated has an OH-grid topology around the blade, reverting to an H-grid topology further away from it. The wall refinement has an average $y+$ of 25, found to be adequate given that wall functions are used for the boundary-layer resolution. A total of 60 blocks are created, as shown in Fig. 4, totaling 1.2 million cells, and the simulations are run on a cluster using 16 processors.

The inlet boundary conditions are absolute tangential velocity fixed and pressure extrapolated from the interior, as described in Eq. (10). The exit static pressure is held fixed according to Eq. (11). All solid walls are considered impermeable with a no-slip condition. The remaining faces are either block-to-block interfaces or periodic.

Two functions of interest are used: absolute total pressure ratio and isentropic efficiency. The absolute total pressure ratio is defined as

$$\pi = \frac{p_{\mathrm{Ta}}^{\mathrm{exit}}}{p_{\mathrm{Ta}}^{\mathrm{inlet}}} \tag{15}$$

and the isentropic efficiency is defined as

$$\eta = \frac{(p_{\mathrm{Ta}}^{\mathrm{exit}}/p_{\mathrm{Ta}}^{\mathrm{inlet}})^{(\gamma-1)/\gamma} - 1}{(T_{\mathrm{Ta}}^{\mathrm{exit}}/T_{\mathrm{Ta}}^{\mathrm{inlet}}) - 1} \tag{16}$$

where the pressure is enthalpy averaged, the temperature is mass averaged at the inlet or exit sections, and the subscript Ta refers to

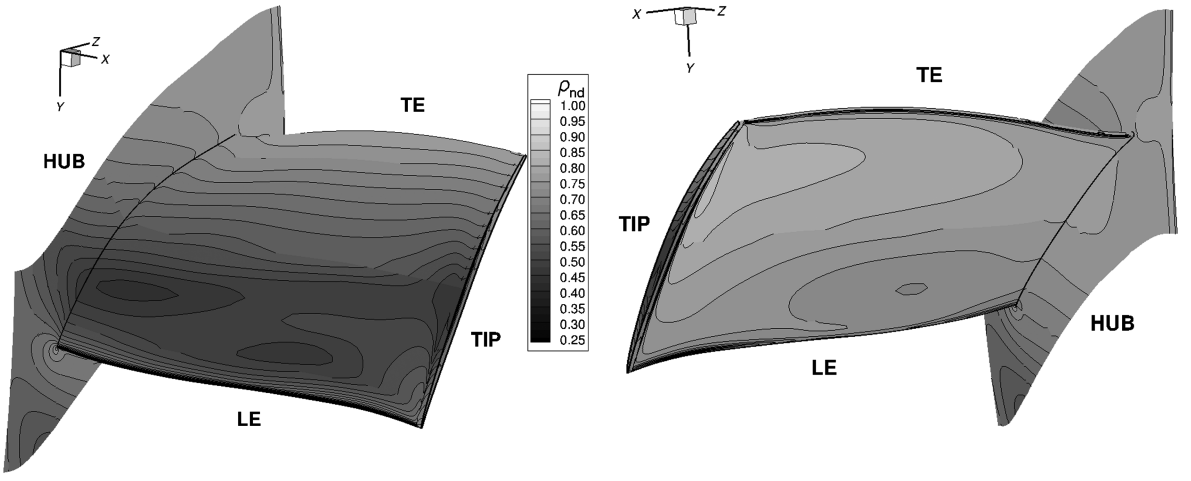

a) Suction side **b) Pressure side**

Fig. 5 Compressor rotor pressure distribution.

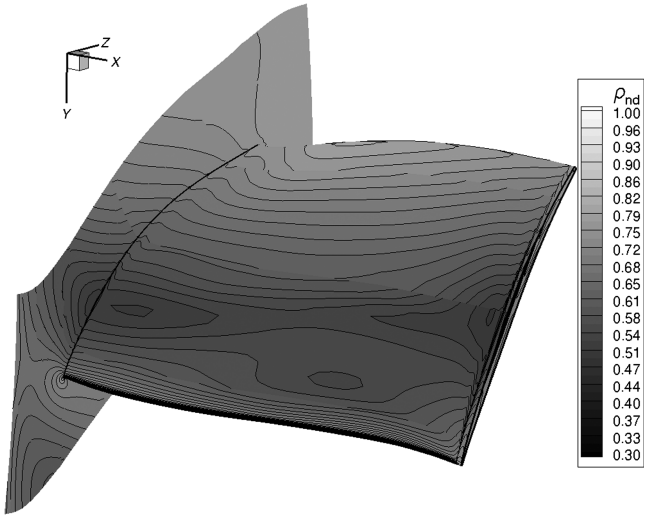

Fig. 6 Compressor rotor density distribution.

a total absolute quantity. For simplicity, these metrics are referred to as pressure ratio and efficiency in the remaining text.

B. Flow and Adjoint Solutions

The flow and adjoint solvers both use a convergence criterion based on the continuity equation residual. Convergence is assumed when the residual relative error reaches 10^{-6}.

The contours of nondimensional pressure on the hub and blade surface planes (suction and pressure sides) are shown in Fig. 5, where the hub, blade tip, leading edge (LE) and trailing edge (TE) are labeled.

The contours of nondimensional density, corresponding to the state variable $q_1 = \rho$ in the solution of Eq. (3), are shown in Fig. 6 on the hub and blade suction side planes.

The contour plots corresponding to the nondimensional adjoint of the continuity equation are shown in Fig. 7 for both functions of interest. These correspond to the adjoint variable $\psi_1 = \psi_\rho$, using the metrics $Y = \pi$ and $Y = \eta$ in the right-hand side for the solution of Eq. (8), and are the adjoint counterpart of the primal solution shown in Fig. 6. Similar to the flow density solution, the two adjoint solutions are only shown on the hub and blade surface planes, despite also being three-dimensional fields. As typical for the adjoint solution, both plots in Fig. 7 show an adjoint flow reversed when compared with the real flow in Fig. 6.

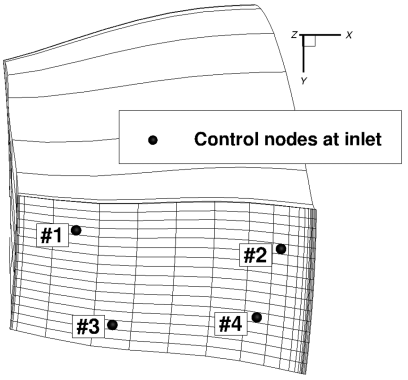

Fig. 8 Control nodes at the inlet boundary face.

C. Verification of Sensitivities

The adjoint-based sensitivity of pressure ratio and efficiency with respect to several inlet boundary conditions are evaluated using Eq. (9).

The adjoint-based sensitivities are verified against first-order forward-difference derivative approximations. The formula for the first derivative, obtained from the Taylor series expansion of function Y for a perturbation about a point u, is used

$$\frac{\mathrm{d}Y}{\mathrm{d}u} = \frac{Y(u + \Delta u) - Y(u)}{\Delta u} + O(\Delta u) \tag{17}$$

Although a second-order FD approximation would have been preferred to minimize the truncation error, its computational cost would have been doubled because twice the CFD runs are needed.

The verification runs are made using coarser grids to mitigate the computational effort required by FD. Regarding the inlet BC sensitivity verification, the mesh is coarsened two levels and four inlet face nodes are selected, as illustrated in Fig. 8. For the exit BC sensitivity verification, only one level coarsening is used, and four exit face nodes are selected, as illustrated in Fig. 9.

The verification is made by forcing a variation in the prescribed BC parameter at each of these control nodes. Because the flow solver is only prepared to read boundary radial profiles, it is necessary to modify the code after these have been read to perturb the boundary face value at the selected control nodes. This implies running separately the flow solver to convergence over and over again for each parameter, for each node, which equates to a total of 24 times, corresponding to the five prescribed inlet parameters ($p_T^{\text{inlet}}, h_T^{\text{inlet}}, V_t^{\text{inlet}}, C_r^{\text{inlet}}, C_z^{\text{inlet}}$) at the four inlet control nodes, and

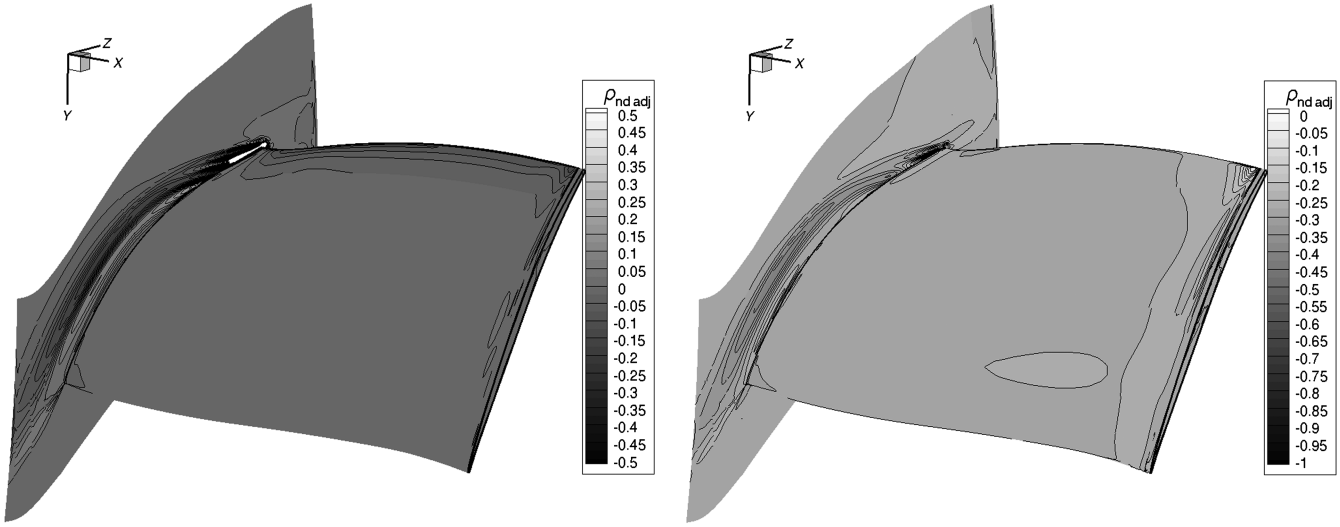

a) Pressure ratio ($Y = \pi$) **b) Effciency ($Y = \eta$)**

Fig. 7 Compressor rotor adjoint solution of the continuity equation.

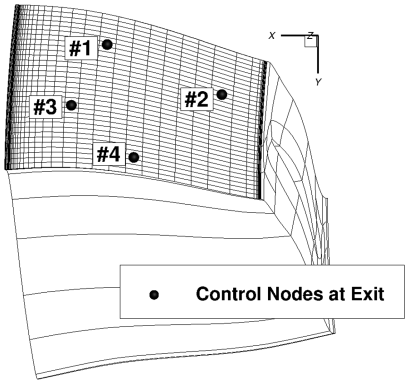

Fig. 9 Control nodes at the exit boundary face.

the prescribed exit parameter p^{exit} at the four exit control nodes. In practice, a much higher number of runs are necessary because the expression (17), as any FD derivative approximation, suffers from a large sensitivity to the choice of step size Δu. If the perturbation is chosen too large, the derivative estimate might be inaccurate because of the large truncation error; if it is made too small, then subtractive cancellation might occur and the estimate is again inaccurate. After some trials, the sweet spot of Δu is found to be 0.25% for p_T^{inlet}, 1% for h_T^{inlet}, 3% for V_t^{inlet}, and 0.5% for p^{exit}.

The comparison between the adjoint-based sensitivities and the FD derivative approximation with respect to the inlet total pressure, enthalpy, and absolute tangential velocity is summarized in Figs. 10–12, respectively, for the inlet boundary face nodes shown in Fig. 8. The errors are computed using the RANS adjoint-based sensitivity values as reference.

Considering that first derivatives are being compared, not function values, and taking into account the strong sensitivity to the perturbation step Δu experienced by the finite differences, there is a very good agreement between the RANS adjoint-based sensitivities and the FD derivative approximations for the tested node locations. Even in cases where the relative difference is higher, not only do the values have the same sign (which indicates a consistent direction of change of the evaluated metric function with respect to the design parameter), but also their absolute values remain very close. These results demonstrate the correct implementation of the inlet BC sensitivity assessment.

Perturbing the exit pressure at the boundary face nodes shown in Fig. 9 produces the comparison between the adjoint-based sensitivities and the FD derivative approximation summarized in Fig. 13. Again, there is a good match between the two sensitivity analysis methods, proving once again the adjoint approach.

The fact that the full RANS adjoint is being used, that is, all terms have been linearized in the adjoint formulation (from artificial dissipation to eddy viscosity), implies that the discrepancies between the adjoint-based and the finite difference gradients are mainly due to numerical errors in the latter. This comes as no surprise because not only a first-order finite difference gradient approximation is used, but also a rather high sensitivity to the perturbation step size Δu in Eq. (17) has been experienced.

D. Performance Sensitivity to Inlet Conditions

Five different inlet BC parameters are analyzed: inlet total pressure p_T^{inlet}, inlet total enthalpy h_T^{inlet} (computed from inlet total

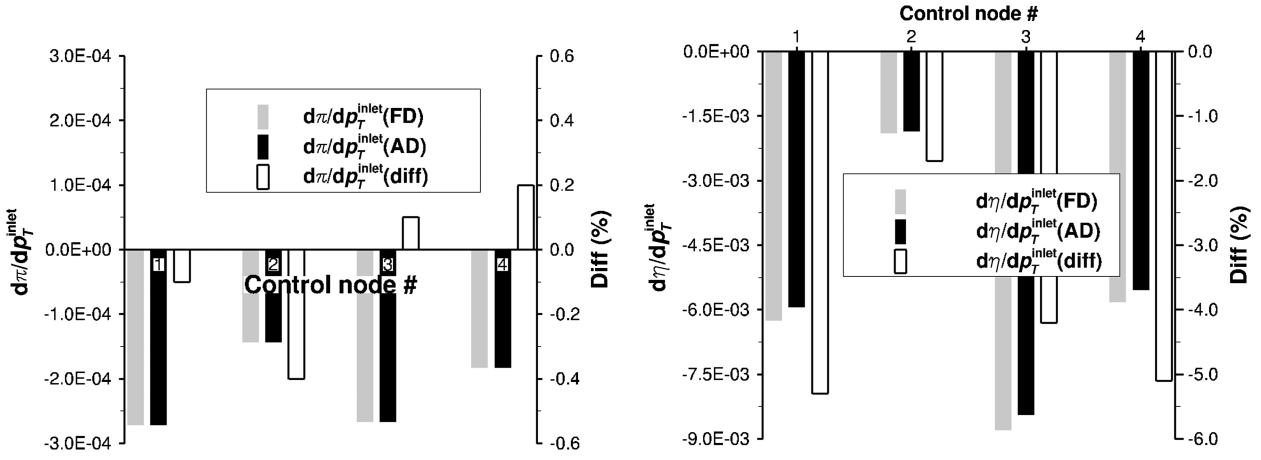

a) Pressure ratio ($Y = \pi$) b) Effciency ($Y = \eta$)

Fig. 10 Verification of adjoint-based sensitivity with respect to p_T^{inlet} using FD.

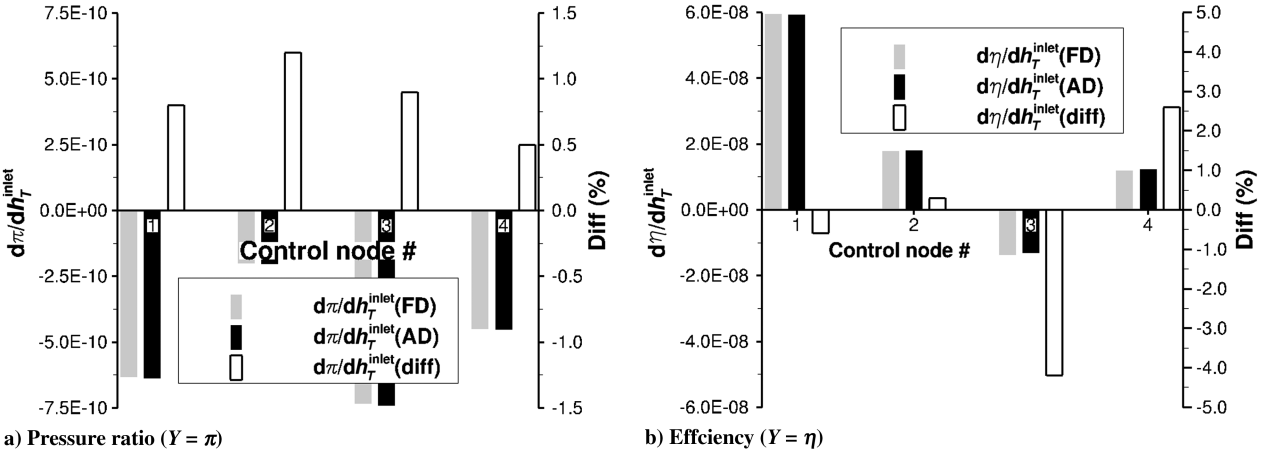

a) Pressure ratio ($Y = \pi$) b) Effciency ($Y = \eta$)

Fig. 11 Verification of adjoint-based sensitivity with respect to h_T^{inlet} using FD.

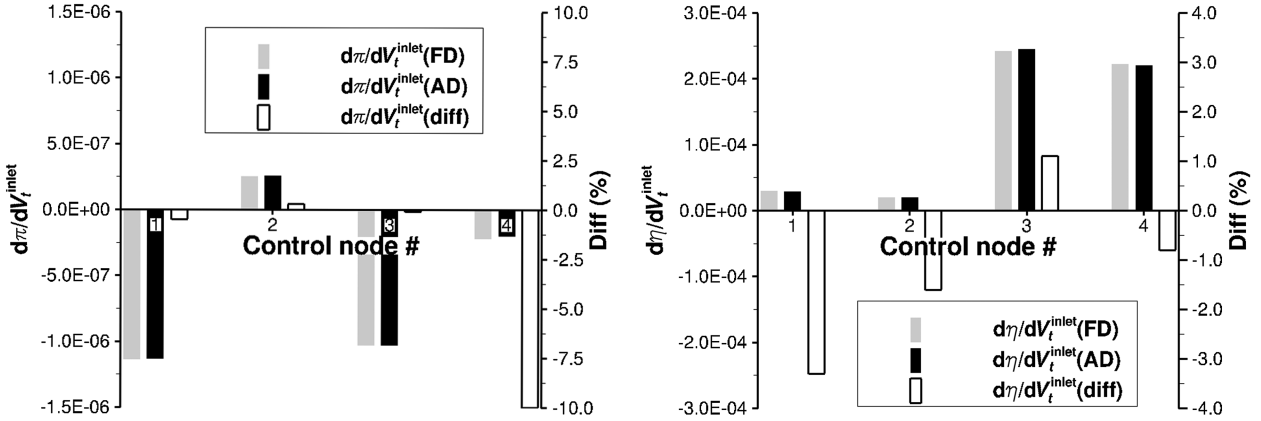

a) Pressure ratio ($Y = \pi$) b) Effciency ($Y = \eta$)

Fig. 12 Verification of adjoint-based sensitivity with respect to V_t^{inlet} using FD.

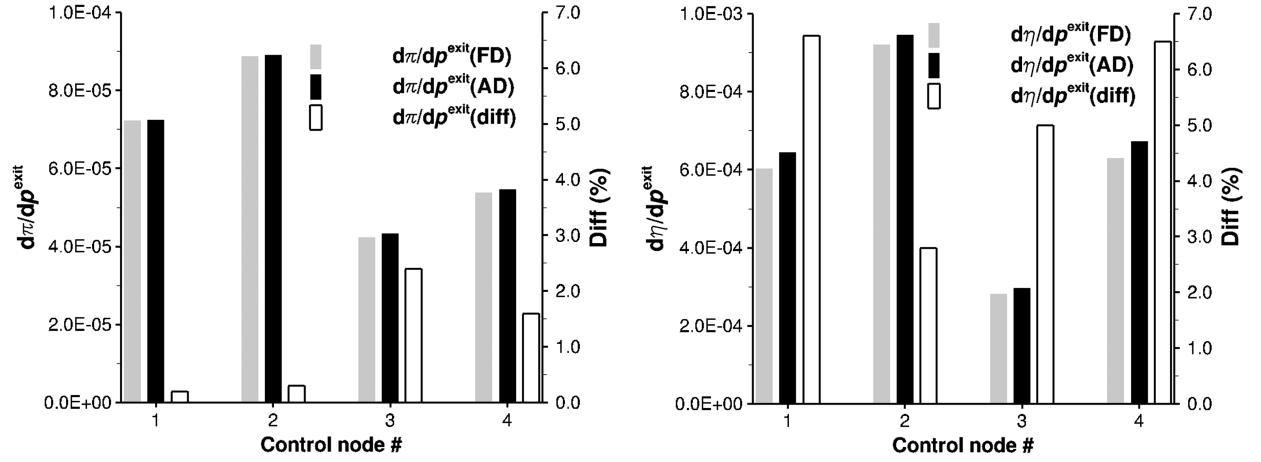

a) Pressure ratio ($Y = \pi$) b) Effciency ($Y = \eta$)

Fig. 13 Verification of adjoint-based sensitivity with respect to p^{exit} using FD.

temperature), absolute tangential velocity V_t^{inlet}, and radial C_r^{inlet} and axial C_z^{inlet} direction cosines.

A positive value at a point indicates the increased magnitude of pressure ratio π or efficiency η per unit change in the inlet boundary condition parameter at that boundary face node. Consequently, a designer can easily infer from Figs. 14–22 how sensitive the blade performance is to these inlet boundary conditions.

Besides the two-dimensional sensitivity contour plots, the circumferential area average is computed and plotted together with the boundary condition area-averaged profile set in the test case. The BC

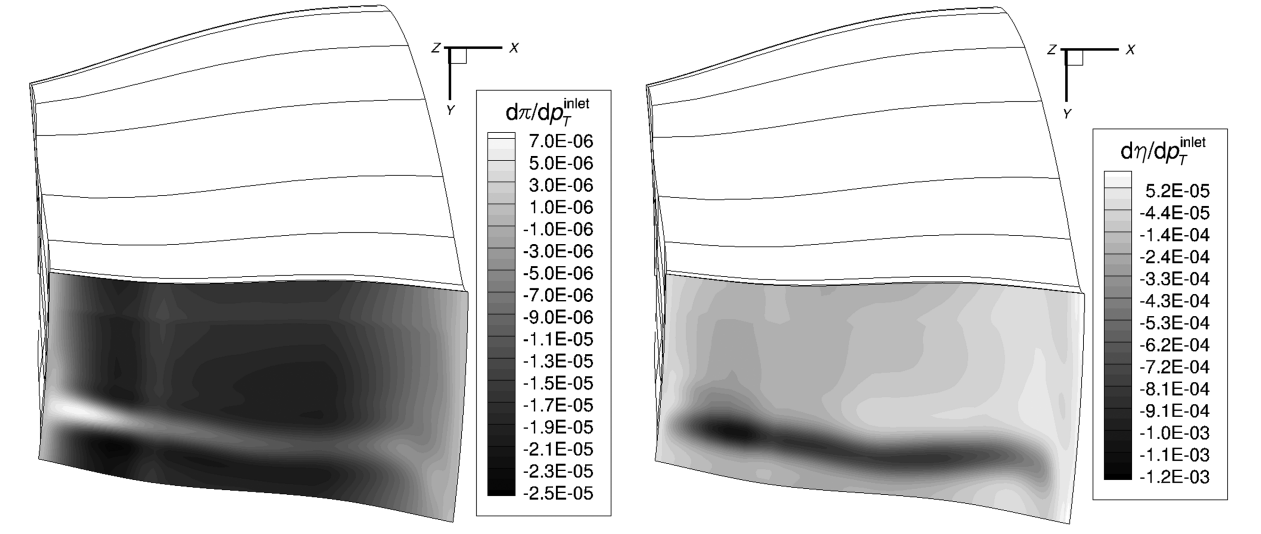

a) Pressure ratio ($Y = \pi$) b) Effciency ($Y = \eta$)

Fig. 14 Compressor rotor efficiency and pressure ratio sensitivity with respect to inlet total pressure.

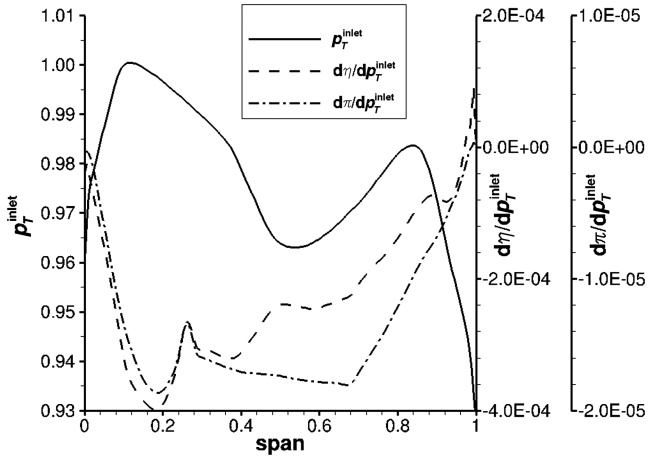

Fig. 15 Compressor rotor efficiency and pressure ratio sensitivity with respect to circumferentially averaged inlet total pressure.

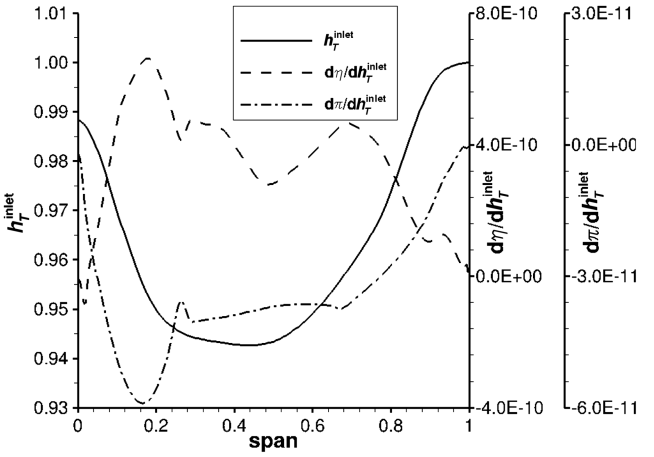

Fig. 17 Compressor rotor efficiency and pressure ratio sensitivity with respect to circumferentially averaged inlet total enthalpy.

profiles of p_T^{inlet}, h_T^{inlet}, and V_t^{inlet} were nondimensionalized using their maximum values as reference. In those one-dimensional plots, the span variable in the horizontal axis ranges from zero (hub) to one (casing).

For the computational mesh used, the inlet boundary has a total of 5376 cell faces. Because one single run of the adjoint-based solver evaluates the sensitivity of one performance parameter with respect to the number of BC parameters times this number of boundary cell faces, this means that a total of 26,880 sensitivity values are evaluated by the solver.

The sensitivity of the performance metrics with respect to the inlet total pressure is shown in Figs. 14 and 15. The former figure shows the sensitivity in the two-dimensional inlet plane. The latter figure shows the circumferentially averaged values of the sensitivities. The circumferentially averaged profiles of the sensitivities shows that, in general, if the total pressure profile is made more uniform, then it can improve the efficiency of the rotor. In particular, it can be noticed that, near the endwalls, the effect of increasing the total pressure is an attempt to decrease the viscous effects from the walls. This suggests that improvements on the upstream stator or the endwall design are one way to achieve this uniform pressure profile going into the rotor. In the two-dimensional plots for the sensitivity, a region of strong total pressure gradients at around the 20 and 80% span can be observed. In this region, the sensitivity plots suggest a decrease in the total pressure. In addition, the effect of the blade can be seen as a streak at the inlet plane, along which a decrease in total pressure increases the efficiency of the rotor.

The influence of the inlet total absolute enthalpy is presented in Figs. 16 and 17. As in the plots for the sensitivity for total pressure, the plots for sensitivity to total temperature suggest that an overall uniform inlet total enthalpy will increase the efficiency of the rotor. Hence, a decrease in the total enthalpy near the endwalls, leading to local smaller total temperatures, enables all portions of the rotor to be equally (and more) effective in pumping the flow to the downstream blade row. One way to achieve this is through improved blade and endwall design that reduces friction losses. In the middle of the inlet plane, the sensitivities suggest that (as expected) reducing the mixing losses from the wake of the upstream blade row is one possible way to increase the efficiency of the rotor. Relative to the gains from altering the profile near the endwalls, altering the profile in the core of the flow seems to have a bigger impact on the overall efficiency. It is interesting to note that the sensitivities of the inlet total enthalpy to the efficiency and the pressure ratio are in opposite (and roughly equal magnitude) directions.

In Figs. 18 and 19, the effect of the inlet absolute tangential velocity on the blade rotor performance is illustrated. The contours on the two-dimensional plot again show a region of large changes that corresponds to the portion of the flow incident on the leading edge of

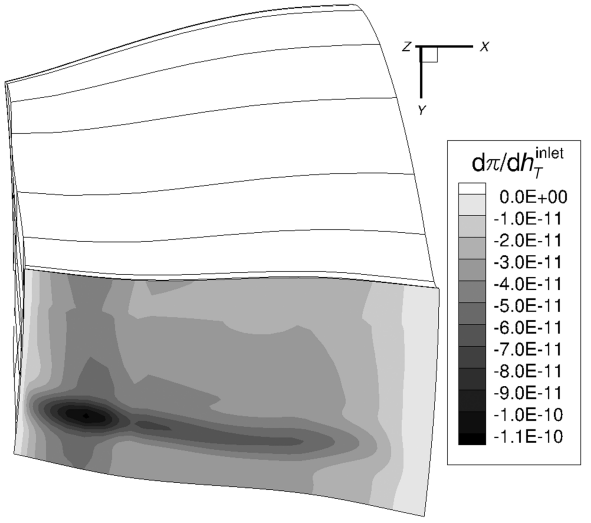

a) Pressure ratio ($Y = \pi$)

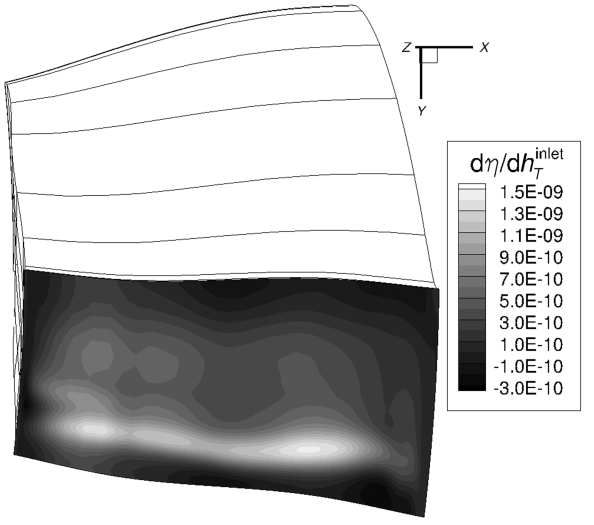

b) Effciency ($Y = \eta$)

Fig. 16 Compressor rotor efficiency and pressure ratio sensitivity with respect to inlet total enthalpy.

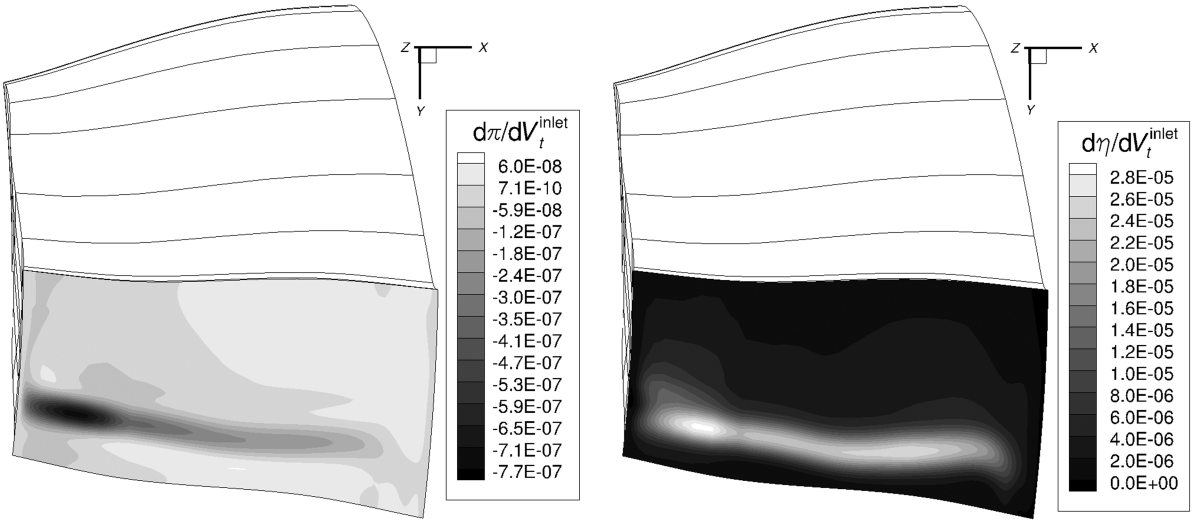

a) Pressure ratio ($Y = \pi$) **b) Effciency ($Y = \eta$)**

Fig. 18 Compressor rotor efficiency and pressure ratio sensitivity with respect to inlet absolute tangential velocity.

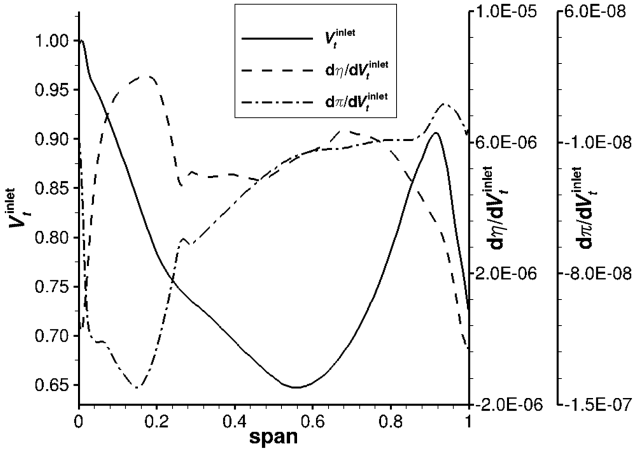

Fig. 19 Compressor rotor efficiency and pressure ratio sensitivity with respect to circumferentially averaged inlet absolute tangential velocity.

the blade. The circumferentially averaged profiles in Fig. 19 show changes to the tangential velocity that are mostly positive and suggest sharp changes near the hub. To improve the efficiency, this averaged profile needs to be decreased, thus suggesting that the blade may be in an off-incidence condition. This could be due to the endwall three-dimensional effects. The region between the 20 and 80% span shows an overall constant increase in tangential velocity. However, in the tip region, the changes decrease rapidly to zero (or small negative numbers), suggesting that the blade is at the correct incidence while accounting for tip flow features. It is interesting to note that the changes to the profile for improvements in efficiency and pressure ratio are in different directions in the bottom (<40% span) and tip portions of the blade.

The performance sensitivity to the inlet radial and axial direction cosines are shown in Figs. 20–23. Unlike the tangential velocity profiles, there is no discernible effect of endwalls and tip effects here. The circumferentially averaged plots indicate that where the radial direction cosines are positive there is a suggested reduction and where it is negative there is a suggested increase. This trend is the same for both efficiency and pressure ratio. This suggests that,

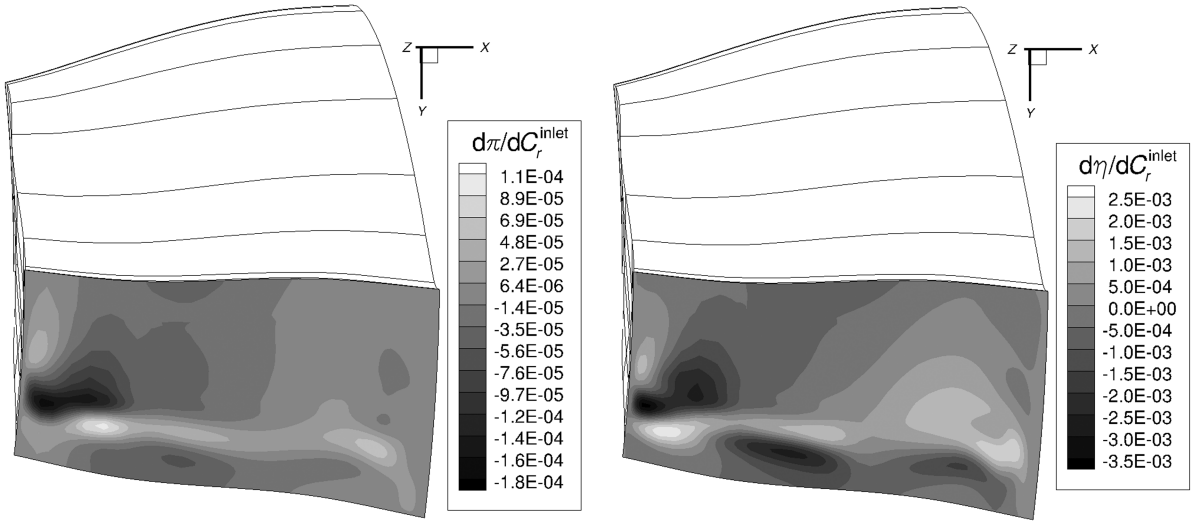

a) Pressure ratio ($Y = \pi$) **b) Effciency ($Y = \eta$)**

Fig. 20 Compressor rotor efficiency and pressure ratio sensitivity with respect to inlet radial direction cosine.

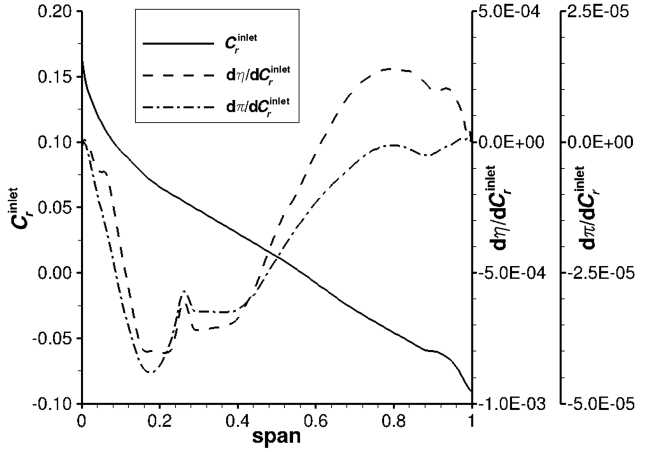

Fig. 21 Compressor rotor efficiency and pressure ratio sensitivity with respect to circumferentially averaged inlet radial direction cosine velocity.

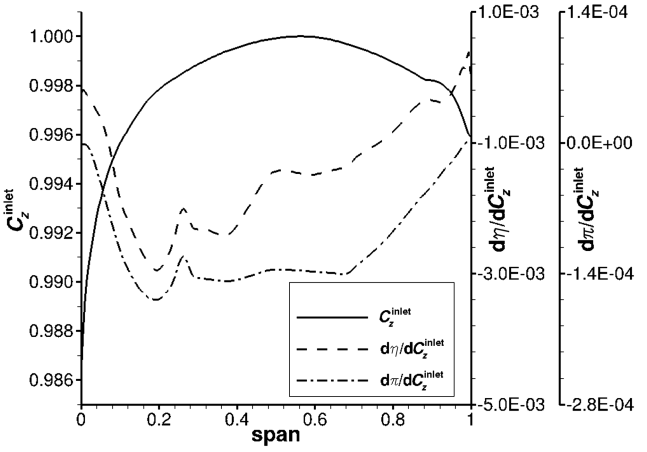

Fig. 23 Compressor rotor efficiency and pressure ratio sensitivity with respect to circumferentially averaged inlet axial direction cosine velocity.

overall, the effect of three dimensionality (due to radial shifts) has been accounted for in the baseline design and further improvements can be obtained by small changes.

E. Performance Sensitivity to Exit Conditions

The sensitivity of pressure ratio and efficiency with respect to exit boundary conditions are shown in Figs. 24 and 25. Similar to the inlet condition plots, a positive value at a point indicates the increased magnitude of pressure ratio π or efficiency η per unit change in the exit boundary condition parameter at that boundary face node. In Fig. 25, the profile of p^{exit} was nondimensionalized using its maximum value as reference.

The suggested changes to the exit static pressure for improvement in efficiency (Figs. 24 and 25) are consistent with the definition of efficiency. It is interesting to note that a larger increase in static pressure is suggested near the root region (<20% span). The overall increase in static pressure at the exit for a fixed velocity leads to a larger exit total pressure, suggesting that the rotor is more efficient. The suggested changes also lead to a flatter exit pressure profile and, recalling the turbomachinery radial equilibrium equation, this can be achieved by controlling the circumferential velocity distribution (swirl). One way to obtain this is by reducing the flow turning and profile losses on the rotor in the midpassage section. The changes to exit pressure that lead to higher pressure ratio π is similar to the profile for the improvements for efficiency. However, the changes are larger in the mid to tip region than the suggested changes for increased efficiency.

F. Example of Tuning Using Sensitivity to Boundary Conditions

As mentioned before, the data produced by using the adjoint-based sensitivity analysis presented in Secs. IV.D and IV.E can be used to improve the blade performance. Such improvement can be achieved by numerical optimization, in particular, using gradient-based optimization algorithms, or by manual tuning, where the designer carefully adjusts the inlet and exit boundary conditions by considering the interaction with the upstream and downstream turbomachinery rows or stages.

To verify and demonstrate the sensitivity information obtained by means of the adjoint method, two simple examples are presented here, in which the inlet and exit boundary conditions are modified compared with the original conditions. The changes follow the sensitivity of pressure ratio and efficiency as given by the previously described adjoint method.

The first example aims to show an improvement of pressure ratio with respect to inlet absolute tangential velocity tuning. The baseline inlet absolute tangential velocity profile (see Fig. 19) is modified by adding the gradient vector as

$$\tilde{V}_t^{\text{inlet}}(s) = V_t^{\text{inlet}}(s) + \alpha \frac{\partial \pi}{\partial V_t^{\text{inlet}}}(s) \tag{18}$$

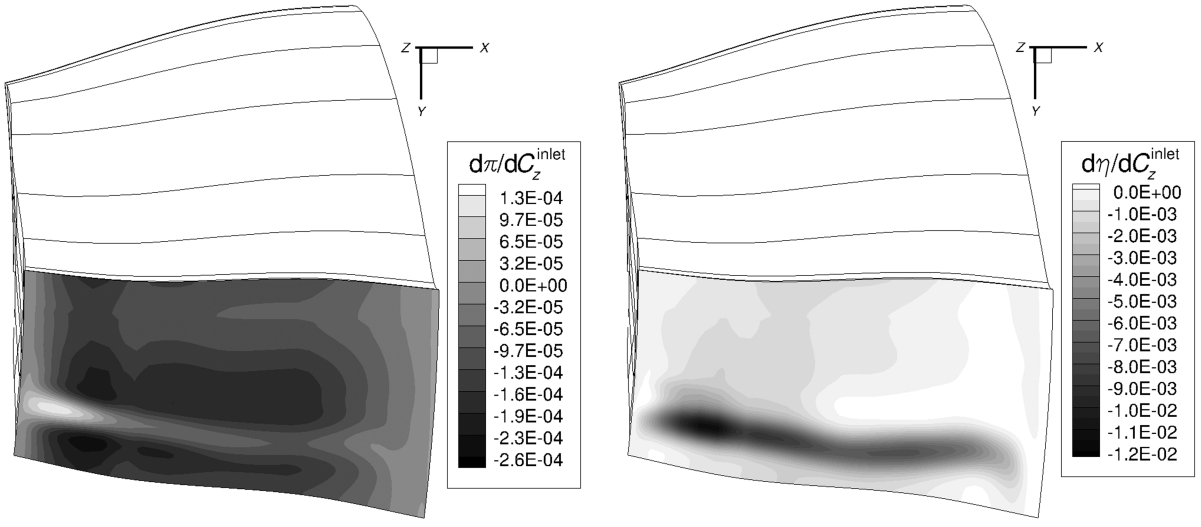

a) Pressure ratio ($Y = \pi$) **b) Effciency ($Y = \eta$)**

Fig. 22 Compressor rotor efficiency and pressure ratio sensitivity with respect to inlet axial direction cosine.

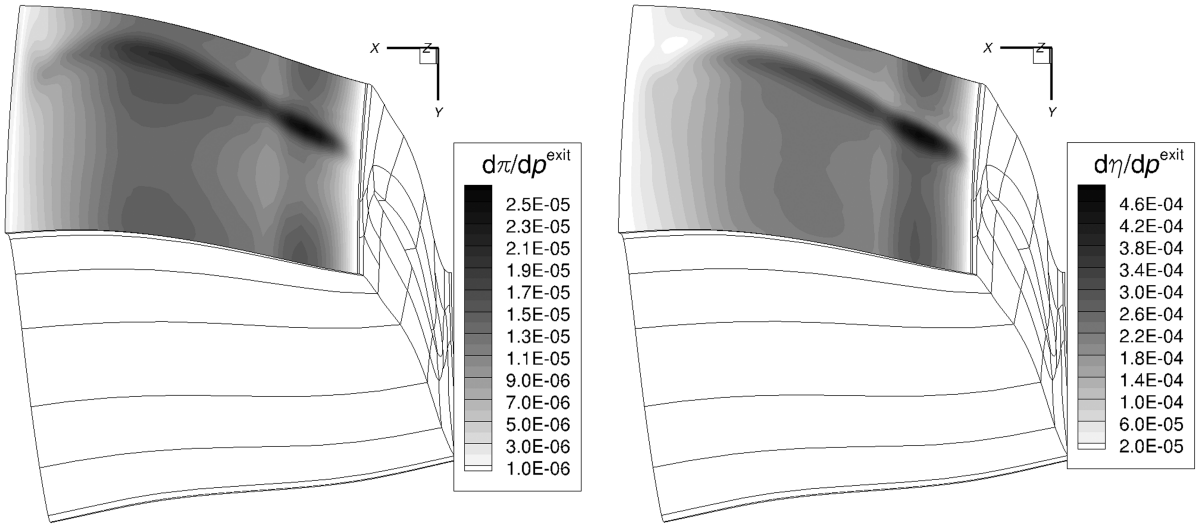

a) Pressure ratio ($Y = \pi$) **b) Effciency ($Y = \eta$)**

Fig. 24 Compressor rotor performance sensitivity with respect to exit static pressure.

where the step α is chosen such that a maximum perturbation of -1% is obtained, resulting in the profile shown in Fig. 26a. As seen from Fig. 26b, a relative improvement of about 0.01% in the pressure ratio is obtained with such modified inlet profile.

The second example shows an improvement of isentropic efficiency with respect to exit static pressure tuning. The baseline exit static pressure profile (see Fig. 25) is modified by adding the gradient vector as

$$\tilde{p}^{\text{exit}}(s) = p^{\text{exit}}(s) + \beta \frac{\partial \eta}{\partial p^{\text{exit}}}(s) \tag{19}$$

where the step β is chosen such that a maximum perturbation of $+1\%$ is obtained, resulting in the profile shown in Fig. 27a. Again, an improvement in the isentropic efficiency is obtained, of about 0.1% in relative terms, as illustrated in Fig. 27b.

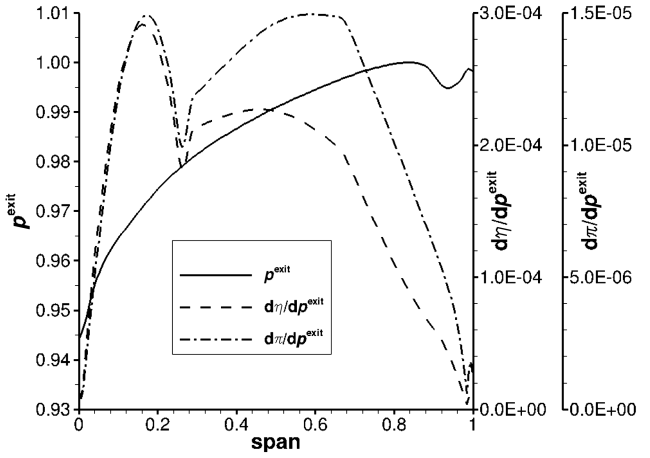

Fig. 25 Compressor rotor efficiency and pressure ratio sensitivity with respect to circumferentially averaged exit static pressure.

V. Conclusions

The control theory has been successfully extended to assess the sensitivity of turbomachinery performance with respect to inlet or exit boundary conditions. The adjoint method approach has been applied to the RANS equations with the k-ω turbulence model, but its implementation can be extended to any set of flow-governing equations.

A realistic compressor rotor blade test case was used to demonstrate the methodology and implementation. The computed sensitivities of efficiency and pressure ratio with respect to some inlet and exit boundary condition parameters proved to be physically correct. The circumferentially averaged profiles of the sensitivities showed that, in general, if the total pressure and total temperature profiles are made more uniform, then they can improve the efficiency

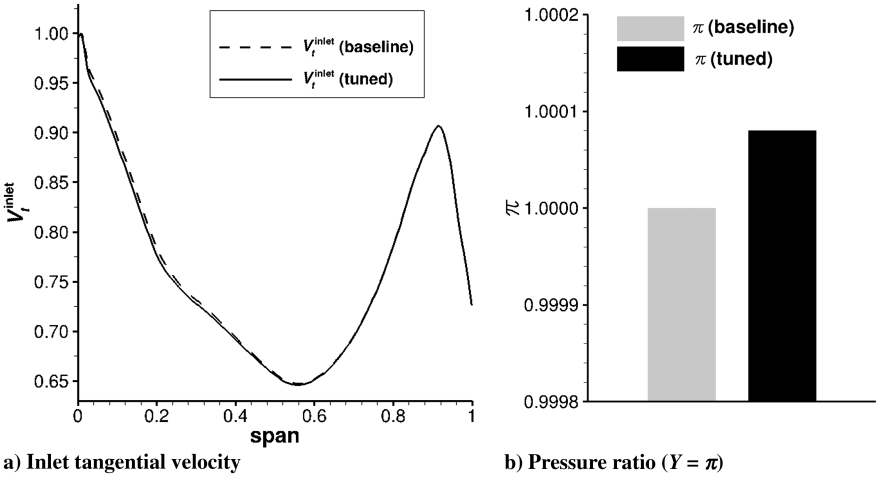

a) Inlet tangential velocity **b) Pressure ratio ($Y = \pi$)**

Fig. 26 Example of tuning of inlet tangential velocity for pressure ratio improvement.

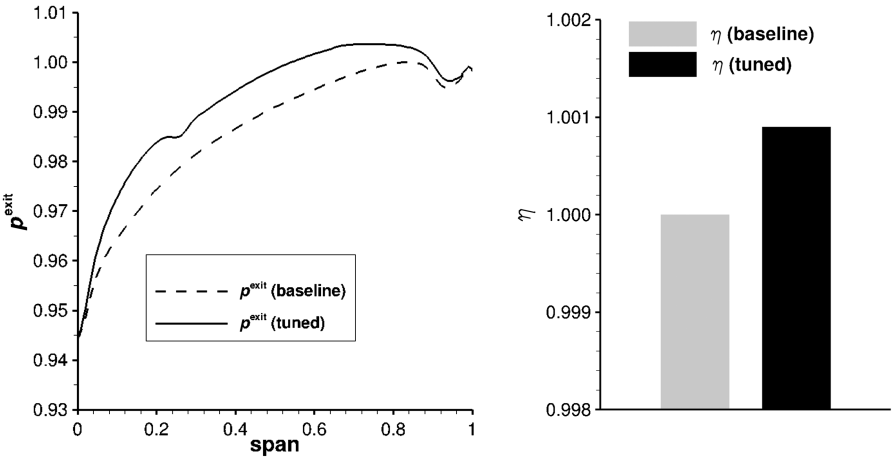

a) Exit static pressure **b) Effciency ($Y = \eta$)**

Fig. 27 Example of tuning of exit static pressure for efficiency improvement.

of the rotor. The produced results also showed important details about endwall viscous effects and blade upstream influence. The effect of the inlet absolute tangential velocity revealed not only significant endwall effects but also tip effects, in a quantitative manner, on the blade rotor performance. The suggested changes to the exit static pressure for improvement in efficiency were also consistent with the definition of efficiency.

The adjoint-based sensitivity of the aerodynamic performance (pressure ratio and efficiency) to inlet total pressure, total enthalpy, inlet absolute tangential velocity, and exit static pressure showed that aerodynamic performance is worse at the endwalls, tip, behind upstream, or current blade row wakes. This is in agreement with the basic physical knowledge of fluid mechanics and turbomachinery, which demonstrate that performance improvements can be made by reducing relative-flow rotationality, or vorticity, by making the flow more uniform.

The use of control theory to assess the sensitivity of turbomachinery performance to boundary conditions proved to be feasible, accurate, and extremely efficient, while providing the designer with valuable information and insights to achieve a robust design. Although the expertise of turbomachinery designers and their incredible insight of the complex physics involved allow them to qualitatively assess the impact of any inlet or exit boundary condition profile change, the adjoint method presented here represents a tool capable of accurately quantifying that impact. In a future outlook, the plethora of information produced by the adjoint approach opens the possibility of incorporating that sensitivity data into a gradient-based design tool, giving the designer the option to produce blades that show greater robustness to varying boundary conditions, such as inlet distortions or ambient conditions.

Acknowledgments

The authors would like to thank Daniel Wilkin, from General Electric Aviation, for his support and feedback. Moreover, the authors are thankful to General Electric for giving permission to publish this paper.

References

[1] Giles, M. B., and Pierce, N. A., "Introduction to the Adjoint Approach to Design," *Flow, Turbulence and Combustion*, Vol. 65, Nos. 3–4, 2000, pp. 393–415. doi:10.1023/A:1011430410075

[2] Pironneau, O., "On Optimum Design in Fluid Mechanics," *Journal of Fluid Mechanics*, Vol. 64, No. 1, 1974, pp. 97–110. doi:10.1017/S0022112074002023

[3] Jameson, A., "Aerodynamic Design via Control Theory," *Journal of Scientific Computing*, Vol. 3, No. 3, 1988, pp. 233–260. doi:10.1007/BF01061285

[4] Jameson, A., Pierce, N. A., and Martinelli, L., "Optimum Aerodynamic Design Using the Navier–Stokes Equations," *Theoretical and Computational Fluid Dynamics*, Vol. 10, Nos. 1–4, 1998, pp. 213–237. doi:10.1007/s001620050060

[5] Martins, J. R. R. A., Alonso, J. J., and Reuther, J. J., "High-Fidelity Aerostructural Design Optimization of a Supersonic Business Jet," *Journal of Aircraft*, Vol. 41, No. 3, 2004, pp. 523–530. doi:10.2514/1.11478

[6] Marta, A. C., and Alonso, J. J., "Toward Optimally Seeded Airflow on Hypersonic Vehicles Using Control Theory," *Computers and Fluids*, Vol. 39, No. 9, 2010, pp. 1562–1574. doi:10.1016/j.compfluid.2010.05.009

[7] Luo, J., Xiong, J., Liu, F., and McBean, I., "Three-Dimensional Aerodynamic Design Optimization of a Turbine Blade by Using an Adjoint Method," *Journal of Turbomachinery*, Vol. 133, No. 1, 2011, Paper 011026. doi:10.1115/1.4001166

[8] Luo, J., Zhou, C., and Liu, F., "Multipoint Design Optimization of a Transonic Compressor Blade by Using an Adjoint Method," *Journal of Turbomachinery*, Vol. 136, No. 5, 2014, Paper 051005. doi:10.1115/1.4025164

[9] Corral, R., and Gisbert, F., "Profiled End Wall Design Using an Adjoint Navier–Stokes Solver," *Journal of Turbomachinery*, Vol. 130, No. 2, 2008, Paper 021011. doi:10.1115/1.2751143

[10] He, L., and Wang, D. X., "Concurrent Blade Aerodynamic-Aero-Elastic Design Optimization Using Adjoint Method," *Journal of Turbomachinery*, Vol. 133, No. 1, 2011, Paper 011021. doi:10.1115/1.4000544

[11] Marta, A. C., Shankaran, S., Venugopal, P., Barr, B., and Wang, Q, "Interpretation of Adjoint Solutions for Turbomachinery Flows," *AIAA Journal*, Vol. 51, No. 7, 2013, pp. 1733–1744. doi:10.2514/1.J052177

[12] Nielsen, E. J., and Diskin, B., "Discrete Adjoint-Based Design for Unsteady Turbulent Flows on Dynamic Overset Unstructured Grids," *AIAA Journal*, Vol. 51, No. 6, 2013, pp. 1355–1373. doi:10.2514/1.J051859

[13] Buckley, H. P., and Zingg, D. W., "Approach to Aerodynamic Design Through Numerical Optimization," *AIAA Journal*, Vol. 51, No. 8, 2013, pp. 1972–1981. doi:10.2514/1.J052268

[14] Leung, T. M., and Zingg, D. W., "Aerodynamic Shape Optimization of Wings Using a Parallel Newton–Krylov Approach," *AIAA Journal*, Vol. 50, No. 3, 2013, pp. 540–550. doi:10.2514/1.J051192

[15] Fidalgo, V. J., Hall, C. A., and Colin, Y., "Study of Fan-Distortion Interaction Within the NASA Rotor 67 Transonic Stage," *Journal of Turbomachinery*, Vol. 134, No. 5, 2012, Paper 051011. doi:10.1115/1.4003850

[16] Wilcox, D. C., "Reassessment of the Scale-Determining Equation for Advanced Turbulence Models," *AIAA Journal*, Vol. 26, No. 11, 1988, pp. 1299–1310. doi:10.2514/3.10041

[17] Holmes, D. G., Mitchell, B. E., and Lorence, C. B., "Three Dimensional Linearized Navier–Stokes Calculations for Flutter and Forced Response," *Unsteady Aerodynamics and Aeroelasticity of Turbomachines*, edited by Fransson, T. H., Vol. 4, Springer, New York, 1998, pp. 211–224. doi:10.1007/978-94-011-5040-8_14

[18] Felten, F. N., Kapetanovic, S., Holmes, D. G., and Ostrowski, M., "Gas Turbine Temperature Prediction Using Unsteady (CFD) and Realistic Non-Uniform (2D) Combustor Exit Properties," *Proceedings of the ASME Turbo Expo 2008: Power for Land, Sea and Air*, ASME International Gas Turbine Inst. Paper GT2008-50275, Berlin, Germany, 2008.
doi:10.1115/GT2008-50275

[19] Holmes, D. G., "Mixing Planes Revisited: A Steady Mixing Plane Approach Designed to Combine High Levels of Conservation and Robustness," *Proceedings of the ASME Turbo Expo 2008: Power for Land, Sea and Air*, American Society of Mechanical Engineers Paper GT2008-51296, June 2008.
doi:10.1115/GT2008-51296

[20] Marta, A. C., Mader, C. A., Martins, J. R. R. A., van der Weide, E., and Alonso, J. J., "Methodology for the Development of Discrete Adjoint Solvers Using Automatic Differentiation Tools," *International Journal of Computational Fluid Dynamics*, Vol. 21, Nos. 9–10, 2007, pp. 307–327.
doi:10.1080/10618560701678647

[21] Pascual, V., and Hascoët, L., "Extension of TAPENADE Towards Fortran 95," *Automatic Differentiation: Applications, Theory, and Tools*, edited by Bücker, H. M., Corliss, G., Hovland, P., Naumann, U., and Norris, B., Vol. 50, Lecture Notes in Computational Science and Engineering, Springer, New York, 2006, pp. 171–179.
doi:10.1007/3-540-28438-9

[22] Balay, S., Buschelman, K., Eijkhout, V., Gropp, W. D., Kaushik, D., Knepley, M. G., McInnes, L. C., Smith, B. F., and Zhang, H., "PETSc Users Manual," Argonne National Lab., TR ANL-95/11, Rev. 2.3.0, Argonne, IL, 2004.

[23] Marta, A. C., Shankaran, S., Holmes, D. G., and Stein, A., "Development of Adjoint Solvers for Engineering Gradient-Based Turbomachinery Design Applications," *Proceedings of the ASME Turbo Expo 2009: Power for Land, Sea and Air*, American Society of Mechanical Engineers Paper GT2009-59297, 2009.
doi:10.1115/GT2009-59297

[24] Marta, A. C., and Shankaran, S., "On the Handling of Turbulence Equations in RANS Adjoint Solvers," *Computers & Fluids*, Vol. 74, No. 30, 2013, pp. 102–113.
doi:10.1016/j.compfluid.2013.01.012

F. Liu
Associate Editor